MoS_2 Polymorphic Engineering Enhances Selectivity in the Electrochemical Reduction of Nitrogen to Ammonia

Bryan H. R. Suryanto,[#,1] Dabin Wang,[#,1] Luis Miguel Azofra,[2*] Moussab Harb,[2] Luigi Cavallo,[2] Rouhollah Jalili,[3] David R. G. Mitchell,[4] Manjunath Chatti,[1] and Douglas R. MacFarlane[1*]*

[1] Australian Centre for Electrochemical Science,School of Chemistry, Monash University Clayton, VIC 3800 (Australia).

[2] KAUST Catalysis Centre (KCC),King Abdullah University of Science and Technology (KAUST) Thuwal, 23955-6900 (Saudi Arabia).

[3] School of Science, RMIT University, Melbourne, VIC 3001 (Australia)

[4] UOW Electron Microscopy Centre, University of Wollongong, Wollongong, NSW 2522 (Australia).

***Corresponding authors:**

bryan.suryanto@monash.edu; luis.azoframesa@kaust.edu.sa; douglas.macfarlane@monash.edu.

ABSTRACT

The electrochemical N_2 reduction reaction (NRR) offers a direct pathway to produce NH_3 from renewable energy. However, aqueous NRR suffers from both low Faradaic efficiency (FE) and yield rate. The main reason is the more favoured H^+ reduction to H_2 in aqueous electrolytes. Here we demonstrate a highly-selective Ru/MoS_2 NRR catalyst on which the MoS_2 polymorphs can be controlled to suppress H^+ reduction. A NRR FE as high as 17.6% and NH_3 yield rate of 1.14×10^{-10} mol cm^{-2} s^{-1} is demonstrated at 50°C. Theoretical evidence supports a hypothesis that the high NRR activity originates from the synergistic interplay between the Ru clusters as N_2 binding sites and nearby isolated S-vacancies on the 2H-MoS_2 as centres for hydrogenation; this supports formation of NH_3 at the Ru/2H-MoS_2 interface.

TOC GRAPHICS

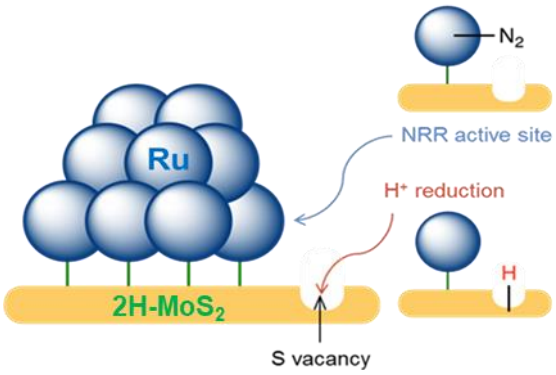

It is reported that the conventional Haber-Bosch process consumes approximately 2% of global energy supply and contributes ~1.5% of global greenhouse gas emissions.[1] Renewable energy powered dinitrogen (N_2) fixation technologies to synthesize ammonia (NH_3) offers a core solution to the energy and environmental challenges caused by the conventional Haber-Bosch process.[2]

The electrochemical nitrogen reduction reaction (NRR) at ambient conditions offers a direct pathway for the conversion of renewable electricity into NH_3 in a simple electrolytic cell.[3] The required H^+ can be sustainably supplied from a water oxidation process[4]. However, the NRR process is kinetically sluggish, involving the addition of $6e^-$ and $6H^+$ and is electrochemically disfavored over the more facile, $2e^-$ and $2H^+$ hydrogen evolution reaction (HER) in aqueous solution.[3, 5] The highly disruptive HER largely explains why most of the recently reported metal based electrocatalysts such as Ru,[6] Pt,[7] Au,[8] Rh,[9] Fe,[10-11] Mo,[12] Pd,[13] Cr,[14] and N-doped carbon based materials[15-16], often suffer from both low NRR Faradaic efficiency of <15% and low NH_3 yield rates in the range of 10^{-11} to 10^{-10} mol cm^{-2} s^{-1}.

Recent efforts are devoted towards the development of NRR electrocatalysts based on rational approaches.[3] Common strategies are the design of inherently active NRR catalysts guided by theoretical calculations and inspired by the nature's nitrogenase enzymes.[17-20] Another design approach is the suppression of HER rates. Since the initial H^+ adsorption to catalytically active sites (*) in the HER process is driven by charge transfer ($H^+ + e^- + * \leftrightarrow *H$), it is proposed that the physical properties of catalyst, substrate and electrolyte are crucial in limiting HER.[3, 21] Our group has proposed novel strategies including the use of aprotic,[22] and ionic liquid,[23] electrolytes to limit HER.

In the present report we demonstrate the impact of HER suppression on the NRR activities of a composite catalyst structure. The MoS_2, which is known for having tunable HER activities,

is decorated with Ru clusters to provide active binding sites for N_2 activation. NRR activity and selectivity is significantly enhanced on 'semiconducting' type Ru decorated 2H-MoS_2 (denoted as Ru/2H-MoS_2) in contrast to that of 'metallic' type 1T-MoS_2. It is demonstrated that the ability to control HER kinetics by tuning MoS_2 properties *via* polymorphic engineering is critical in achieving high NRR activity.

Scanning transmission electron microscopy (STEM) images (Figure 1a, S1) at low magnifications show the typical morphology of the synthesized Ru/MoS_2. The high-resolution images in Figure 1b,c and shows that the bright Ru clusters are amorphous (see Section 2.1. for further discussion). The 1T-MoS_2 phase transformation to 2H-MoS_2 following the hydrothermal treatment was evident in the images, as visualized by the transposed patterns in Figure 1b and 1c. Furthermore, energy dispersive X-ray (EDS) characterization shown in Figure S2 and 1e validates the presence of Ru. Additionally, physical characterizations including X-ray diffraction (XRD) and Raman spectroscopy have been carried out in discussed in Section 2.1 of the Supporting Information (Figure S3).

High-resolution X-ray photoelectron spectroscopy (XPS) of Mo 3*d* and Ru 3*p* (Figure S4) clearly demonstrate the polymorphic transformation process of MoS_2 induced by hydrothermal treatment, while the Ru clusters remain unchanged. Important to note are the S: Mo atomic ratios observed in both Ru/1T-MoS_2 and Ru/2H-MoS_2 were found to be ~1.65, indicating the presence of S-vacancies in the Ru/MoS_2 which is also confirmed with HAADF-STEM shown in Figure S5.[24] The important role of S-vacancies in the initial step of proton absorption of HER has been widely demonstrated in prior literatures. Such H^+-S-vacancy structures can dissociate to hydrogen atoms, $H^\bullet$, to provide the 6 proton coupled electron transfer (PCET) steps of the NRR.[25-27] which will be explained by the density functional theory calculation (DFT, *vide infra*).

The initial NRR activity study of each material was evaluated using an H-cell with a standard three-electrode set-up (Figure 2a, further details are provided in Section 1.1 of the Supporting Information) using controlled potential electrolysis (CPE) experiments. As shown in Figure 2b, Ru/2H-MoS_2 exhibits the highest NH_3 yield rate of 6.7 $\times 10^{-11}$ mol cm^{-2} s^{-1}, almost an order of magnitude higher than that of Ru/1T-MoS_2 (9.6 $\times 10^{-12}$ mol cm^{-2} s^{-1} at -200 mV). The NRR performances of undecorated 2H-MoS_2 and 1T-MoS_2 across the tested potentials are generally very low, with most indophenol tests indicating results comparable to that of the background (Figure S8).

Initial voltammetric verification of NRR on Ru/2H-MoS_2 was carried out by linear sweep voltammetry (LSV). As shown in Figure 2c, a slightly higher cathodic current density is observed within the sweeping potential range of -0.05 to -0.2 V vs RHE under N_2 gas purging compared to that of Ar gas purging. Furthermore, a N_2-Ar gas switching experiment (Figure S9) conducted at -0.15 V vs RHE shows higher cathodic currents by about ~14% when the gas stream was switched from Ar to N_2. An extensive set of control experiments including quantitative $^{15}N_2$ (Figure S10), experiments were carried out as described in section 2.2 of the Supporting Information.

The *j-t* curve in Figure 2d shows the current responses obtained at several cathodic potentials between -50 and -400 mV *vs*. RHE. Figure 2e shows that an NRR selectivity (Faradaic efficiency, FE) of 8.5% ± 0.8% at a NH_3 yield rate of 1.2 ± 0.1 $\times 10^{-11}$ mol cm^{-2} s^{-1} can be obtained at -100 mV *vs* RHE. Consistent with a rapidly increasing rate of NRR compared to HER in this region of potential, the application of a more negative potential of -0.15 V increases the Faradaic efficiency (FE) considerably to 12.2 ± 3.0% (data is mean and standard deviation from n = 4 experiments). In addition, no detectable amount of hydrazine was detected after typical CPE at -150 mV (Figure S11). At this potential, an NH_3 yield rate of 9.1 ± 0.2 $\times 10^{-11}$ mol cm^{-2} s^{-1} is measured. Furthermore, the NRR at -150 mV was confirmed by

replacing the purging gas to Ar. Following an hour of controlled potential electrolysis (CPE), the detected ammonia is comparable to that of the background values (2.4 ± 0.2 nmol ml^{-1}, *n* = 2 experiments, Figure S12). Note that this amount has been subtracted from all quantitative results (NH_3 yield rate and NRR FE) reported later in this study as a background value. At potentials more negative than -0.3 V vs RHE the increased dominance of HER results in significantly increased current density, resulting in concomitant loss of NRR FE and NH_3 yield rate. This phenomenon was further verified using gas chromatography measurement of the produced H_2 (Figure S13).

The effect of temperature on NRR performance was also investigated (Figure 2f, S15) at the optimized potential. As shown in Figure 2f, slight increases in FE and NH_3 yield rate to 17.6% and 1.14×10^{-10} mol cm^{-2} s^{-1} were observed at an electrolysis temperature of 50ºC. Increasing the NRR electrolysis temperature further to 60ºC resulted in significant decrease in both FE and NH_3 yield rate, as expected due to the decreased N_2 solubility and increased HER kinetics in the electrolyte at the higher temperatures. Comparing the Ru/2H-MoS_2 NRR performance with literature data (Table S3, Figure S15) it appears that Ru/2H-MoS_2 is amongst the most efficient in the field (Figure S15).

Additionally, the Ru/2H-MoS_2 is able to maintain a relatively stable NRR catalytic activity, as indicated by the stable current profile in Figure S16. Once steady state is established after ~30 minutes, the yield rises linearly in time (Figure S17b) during a 4-hour continuous electrolysis at -150 mV *vs* RHE; after the fourth hour, a total of 622 ± 34 nmols of NH_3 was recovered. The calculated FE and yield rate in the steady state region of Figure S17 is calculated to be 13.8% with a yield rate of 0.46×10^{-10} mol cm^{-2} s^{-1}. A set of physical characterizations, including Raman spectroscopy (Figure S18), SEM-EDS (Figure S19) and inductively coupled plasma – optical emission spectrometry (ICP-OES, Table S2) were also conducted to verify the physical stability of the catalyst.

LSV was also used to establish the polymorphic correlation of MoS_2 to the HER activity for each of the materials. Figure S20 shows that Ru/1T-MoS_2 exhibits an HER onset overpotential of 49 mV and a Tafel slope of ~66 mV dec^{-1}. In contrast, the LSVs of 1T-MoS_2 reveal an onset overpotential of 233 mV and a Tafel slope of ~153 mV dec^{-1}. Similar trends in HER activities were also observed in the 2H-MoS_2 based samples (phase transformed); 2H-MoS_2 exhibits onset overpotential of 330 mV, while Ru/2H-MoS_2 exhibits an onset overpotential of 187 mV and a Tafel slope of ~145 mV dec^{-1}. Therefore, the form of the MoS_2 critically influences the HER kinetics, both with and without the Ru nanoparticle decoration. One major factor that contributes greatly to this phenomenon is the semiconductivity of 2H-MoS_2, compared to that of 1T-MoS_2.[28] Since the H^+/H_2 redox potential lies above the conduction band (CB) energy level of 2H-MoS_2, which has the effect of inhibiting the rate of HER, as is well-known.[29] Hence, the phase dependent HER activity of MoS_2 can be utilized as a tool to promote NRR to become more competitive against the HER. It is also worth noting that this observation is consistent with the behavior of some previously reported NRR catalysts containing semiconducting materials such as Fe_2O_3, $BiVO_4$, CeO_x and TiO_2.[10, 30-32]

DFT calculations were carried out with an optimized heterostructure and interpretative model (Figure 3a and 3b, further discussions are provided in section 2.4 of the Supporting Information), where hydrogenated S-vacancies provide a fundamental role in the NRR mechanism as the H-provider, since the already formed *H can be transferred directly to nearby bound N_2 or to the nitrogen reduction intermediates; for example $*^{Ru}N_2 + *^{S\text{-}vac}H \rightleftharpoons *^{Ru}N_2H$, with the regeneration of the corresponding S-vacancy for further proton reduction steps. Contrary to what has been described for similar materials,[22, 33] adsorbed N_2H is not a stable species in the minimum energy path when catalyzed by Ru (Figure 3 mid-top). Instead, the hydrogenation of $*N_2$ produces in this case spontaneous cleavage into *N and *NH, being 0.72 eV lower in energy with respect to $*N_2 + *H$.[34]

Once *N + *NH are formed (Figure 3 top), a set of successive hydrogenations occur, in which hydrogen is provided from the S-vacancy. Specifically, the analysis of the minimum energy pathway reveals the preferred formation of the *NH + *NH, $*NH_2$ + *NH, $*NH_2$ + $*NH_2$, and $*NH_3$ + $*NH_2$ species during the second to fifth hydrogenations of the nitrogen intermediates. Generation of the first adsorbed ammonia molecule at $*NH_3$ + $*NH_2$ seems to be the rate-limiting step of the whole process, showing a thermodynamic impediment of +0.33 eV. The final hydrogenation of the remaining $*NH_2$ also exhibits a similar thermodynamics impediment of +0.35 eV.

In conclusion, the present work highlights the importance of catalyst design in achieving a highly active and selective NRR electrocatalyst. It is demonstrated that the semiconducting property of 2H-MoS_2 plays an important role in suppressing the HER rate and therefore improving the NRR selectivity of the Ru/2H-MoS_2. The electrocatalyst exhibits a high FE of 17.6% and NH_3 yield rate of 1.14×10^{-10} mol cm^{-2} s^{-1} at 50°C, rendering Ru/2H-MoS_2 is amongst the most efficient in the field (Figure S15). Both the experimental and theoretical evidence suggest that the NRR is catalyzed at the interface of the Ru clusters as the active N_2 binding sites and the S-vacancy in the 2H-MoS_2 as the active H^+ binding sites. The strategy of using semiconducting materials could therefore be further extended in the research and development of catalytic materials for other reactions that are limited by the HER such carbon dioxide reduction.

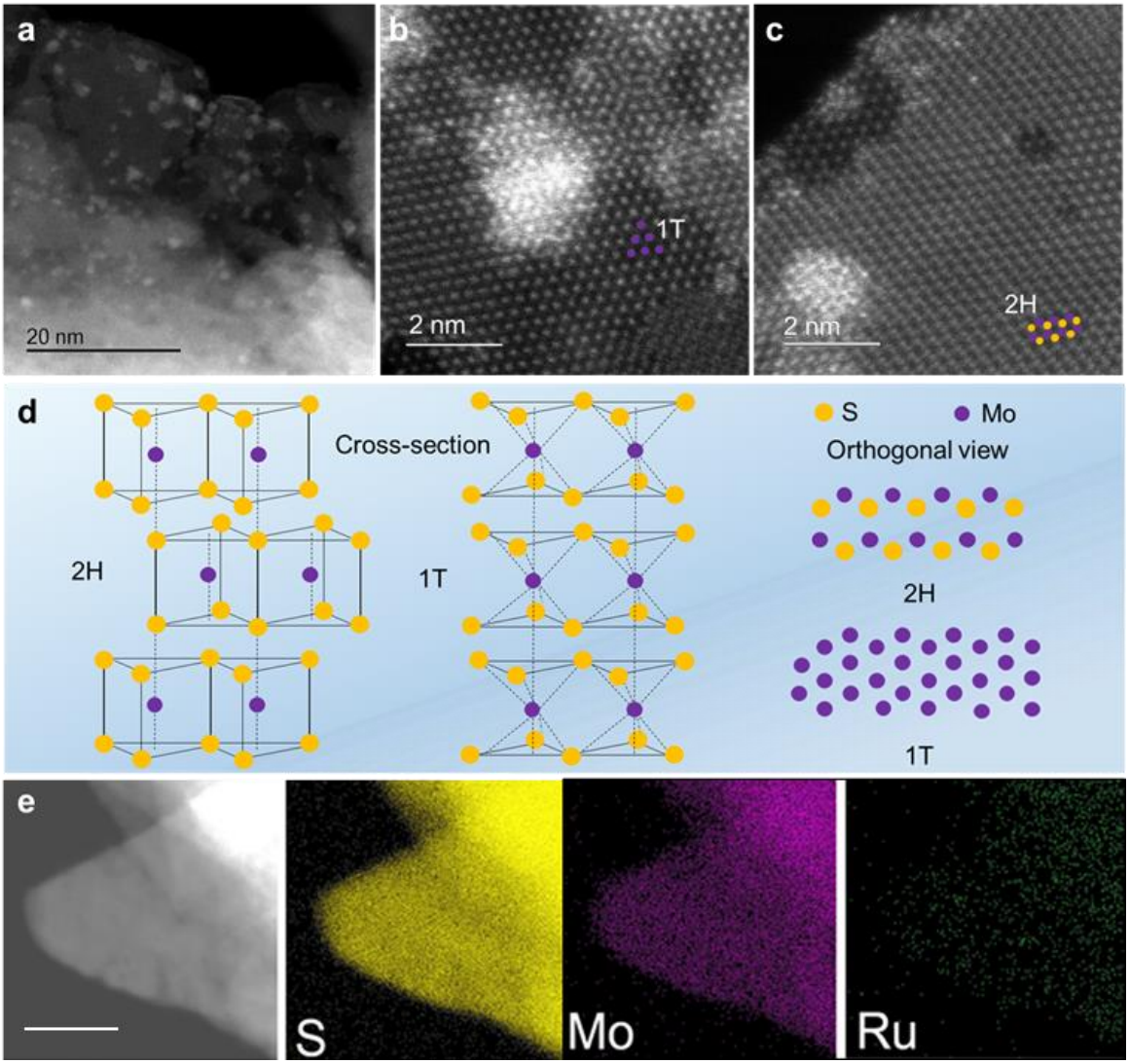

Figure 1. (a) High angle annular dark field (HAADF) – scanning transmission electron microscopy (STEM) images of Ru/2H-MoS_2, High resolution HAADF-STEM imaging of (b) Ru/1T-MoS_2 and (c) Ru/2H-MoS; (d) Schematic illustration of crystallographic difference between 2H and 1T-MoS_2; (e) Energy dispersive X-ray (EDS) elemental mapping (scale bar = 125 nm).

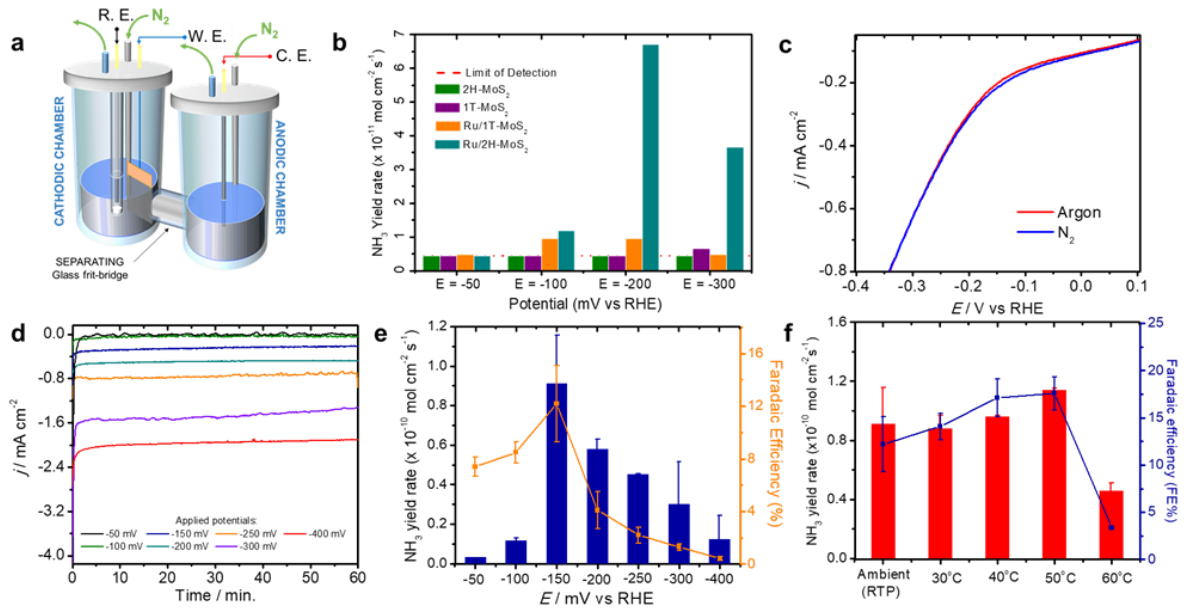

Figure 2. (a) Schematic diagram of the electrochemical cell used for NRR; (b) Nitrogen reduction reaction activity of 2H-MoS_2, 1T-MoS_2, Ru/1T-MoS_2 and Ru/2H-MoS_2 in 10 mM aqueous HCl. (c) Linear sweep voltammograms (LSVs) of Ru/2H-MoS_2 compounds in the presence of nitrogen and argon in 10 mM HCl collected with planar glassy carbon electrode. (d) The corresponding chronoamperometric (*j*-*t*) curves, (e) NRR performance (NH_3 yield rate and Faradaic efficiency) vs. potential (mV) and (f) NRR performance at different electrolysis temperatures at a constant applied potential of -0.15 V vs RHE.

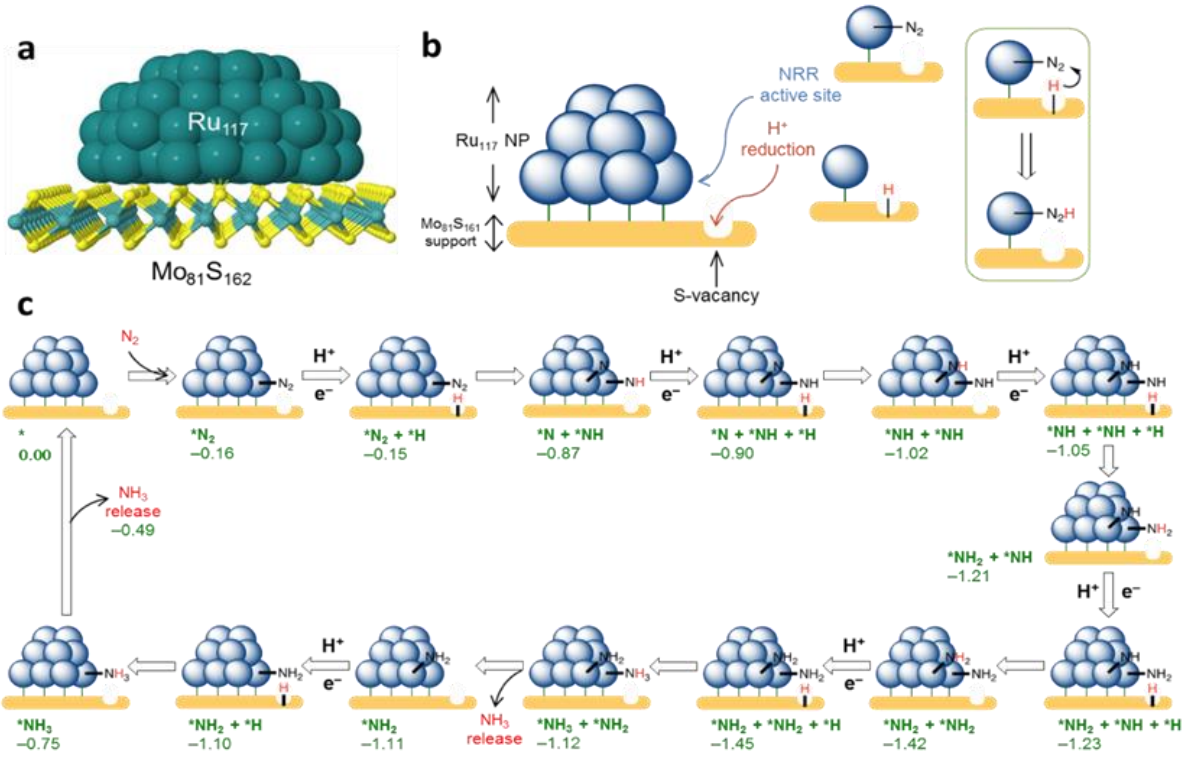

Figure 3. *In-silico* design and electronic properties of Ru/2H-MoS_2 and DFT analysis for NRR mechanism. (a) Initial model consisting in a half-spherical hcp Ru_{117} nanocluster on a perfect 9×9 2H-MoS_2 ($Mo_{81}S_{162}$) pristine supercell; (b) We hypothesize that NRR is catalyzed by Ru/MoS_2 in a synergetic process in which Ru moiety acts as proper NRR active site while S-vacancy on pristine behaves as a HER active site. Once N_2 is adsorbed, a reduced proton on a S-vacancy will subsequently provide hydrogen to N_2 to hydrogenate it; and (c) Schematic minimum energy pathway for the electrochemical N_2 conversion into NH_3 catalyzed by Ru/2H-MoS_2 material. Relative Gibbs free energies are shown in eV at mild conditions (RPBE functional) for the dissociative pathway when there is no applied bias (U = 0 V) and pH = 0. Note: '*' denotes adsorbed species.

AUTHOR INFORMATION

Corresponding Authors

*E-mail: bryan.suryanto@monash.edu; luis.azoframesa@kaust.edu.sa; douglas.macfarlane@monash.edu

Notes

The authors declare no competing financial interests.

ASSOCIATED CONTENT

Supporting Information. Experimental, TEM, XRD, XPS and Raman characterizations, control experiments, $^{15}N_2$ experiments, hydrazine test, gas chromatography, HER performance of Ru/MoS_2, supplementary figures, table of performance, and computational details

Acknowledgements

The authors thank Monash Centre for Electron Microscopy (MCEM) for the provision of access to their instruments. L.M.A. and L.C. acknowledge King Abdullah University of Science and Technology (KAUST) for support. Gratitude is also due to the KAUST Supercomputing Laboratory using the supercomputer Shaheen II for providing the computational resources. This study was supported by an Australian Research Council (ARC) Discovery Grant (DP170102267). D.R.M. is grateful to the ARC for his Australian Laureate Fellowship.

REFERENCES

(1) Licht, S.; Cui, B.; Wang, B.; Li, F.-F.; Lau, J.; Liu, S. Ammonia Synthesis by N_2 and Steam Electrolysis in Molten Hydroxide Suspensions of Nanoscale Fe_2O_3. *Science* **2014,** *345* (6197), 637-640.

(2) Smil, V., Global Population and the Nitrogen Cycle. *Scientific American* **1997,** *277* (1), 76-81.

(3) Singh, A. R.; Rohr, B. A.; Schwalbe, J. A.; Cargnello, M.; Chan, K.; Jaramillo, T. F.; Chorkendorff, I.; Nørskov, J. K. Electrochemical Ammonia Synthesis—The Selectivity Challenge. *ACS Catal.* **2017,** *7* (1), 706-709.

(4) Shipman, M. A.; Symes, M. D. Recent Progress Towards the Electrosynthesis of Ammonia from Sustainable Resources. *Catal. Today* **2017,** *286*, 57-68.

(5) Lee, H. K.; Koh, C. S. L.; Lee, Y. H.; Liu, C.; Phang, I. Y.; Han, X.; Tsung, C.-K.; Ling, X. Y. Favoring The Unfavored: Selective Electrochemical Nitrogen Fixation Using A Reticular Chemistry Approach. *Sci. Adv.* **2018,** *4* (3), eaar3208.

(6) Wang, D.; Azofra, L. M.; Harb, M.; Cavallo, L.; Zhang, X.; Suryanto, B. H. R.; Macfarlane, D. R. Energy-Efficient Nitrogen Reduction to Ammonia at Low Overpotential in Aqueous Electrolyte Under Ambient Conditions. *Chemsuschem* **2018,** *11* (19), 3416-3422.

(7) Yao, Y.; Zhu, S.; Wang, H.; Li, H.; Shao, M. A Spectroscopic Study on the Nitrogen Electrochemical Reduction Reaction on Gold and Platinum Surfaces. *J. Am. Chem. Soc.* **2018,** *140* (4), 1496-1501.

(8) Bao, D.; Zhang, Q.; Meng, F.-L.; Zhong, H.-X.; Shi, M.-M.; Zhang, Y.; Yan, J.-M.; Jiang, Q.; Zhang, X.-B. Electrochemical Reduction of N_2 Under Ambient Conditions for Artificial N_2 Fixation and Renewable Energy Storage Using N_2/NH_3 Cycle. *Adv. Mater.* **2017,** *29* (3), 1604799.

(9) Liu, H.-M.; Han, S.-H.; Zhao, Y.; Zhu, Y.-Y.; Tian, X.-L.; Zeng, J.-H.; Jiang, J.-X.; Xia, B. Y.; Chen, Y. Surfactant-Free Atomically Ultrathin Rhodium Nanosheet Nanoassemblies for Efficient Nitrogen Electroreduction. *J. Mater. Chem. A* **2018,** *6* (7), 3211-3217.

(10) Chen, S.; Perathoner, S.; Ampelli, C.; Mebrahtu, C.; Su, D.; Centi, G. Electrocatalytic Synthesis of Ammonia at Room Temperature and Atmospheric Pressure From Water and Nitrogen on A Carbon-Nanotube-Based Electrocatalyst. *Angew. Chem. Int. Ed.* **2017,** *56* (10), 2699-2703.

(11) Kong, J.; Lim, A.; Yoon, C.; Jang, J. H.; Ham, H. C.; Han, J.; Nam, S.; Kim, D.; Sung, Y.-E.; Choi, J. *et al.* Electrochemical Synthesis of NH_3 at Low Temperature and Atmospheric Pressure Using A Γ-Fe_2O_3 Catalyst. *ACS Sus. Chem. Eng.* **2017,** *5* (11), 10986-10995.

(12) Yang, D.; Chen, T.; Wang, Z., Electrochemical Reduction of Aqueous Nitrogen (N_2) at A Low Overpotential On (110)-Oriented Mo Nanofilm. *J. Mater. Chem. A* **2017,** *5* (36), 18967-18971.

(13) Wang, J.; Yu, L.; Hu, L.; Chen, G.; Xin, H.; Feng, X. Ambient Ammonia Synthesis via Palladium-Catalyzed Electrohydrogenation of Dinitrogen at Low Overpotential. *Nat Commun.* **2018,** *9* (1), 1795.

(14) Zhang, Y.; Qiu, W.; Ma, Y.; Luo, Y.; Tian, Z.; Cui, G.; Xie, F.; Chen, L.; Li, T.; Sun, X. High-Performance Electrohydrogenation of N_2 to NH_3 Catalyzed by Multishelled Hollow Cr_2O_3 Microspheres Under Ambient Conditions. *ACS Catal.* **2018**, *8* (9) 8540-8544.

(15) Liu, Y.; Su, Y.; Quan, X.; Fan, X.; Chen, S.; Yu, H.; Zhao, H.; Zhang, Y.; Zhao, J. Facile Ammonia Synthesis from Electrocatalytic N_2 Reduction Under Ambient Conditions On N-Doped Porous Carbon. *ACS Catal.* **2018,** *8* (2), 1186-1191.
(16) Mukherjee, S.; Cullen, D. A.; Karakalos, S.; Liu, K.; Zhang, H.; Zhao, S.; Xu, H.; More, K. L.; Wang, G.; Wu, G. Metal-Organic Framework-Derived Nitrogen-Doped Highly Disordered Carbon for Electrochemical Ammonia Synthesis Using N_2 and H_2O in Alkaline Electrolytes. *Nano Energy* , **2018,** *48*, 217-226.
(17) Sippel, D.; Rohde, M.; Netzer, J.; Trncik, C.; Gies, J.; Grunau, K.; Djurdjevic, I.; Decamps, L.; Andrade, S. L. A.; Einsle, O. A Bound Reaction Intermediate Sheds Light on the Mechanism of Nitrogenase. *Science* **2018,** *359* (6383), 1484-1489.
(18) Čorić, I.; Mercado, B. Q.; Bill, E.; Vinyard, D. J.; Holland, P. L. Binding of Dinitrogen to an Iron–Sulfur–Carbon Site. *Nature* **2015,** *526*, 96.
(19) Hoffman, B. M.; Lukoyanov, D.; Yang, Z.-Y.; Dean, D. R.; Seefeldt, L. C. Mechanism of Nitrogen Fixation by Nitrogenase: The Next Stage. *Chem. Rev.* **2014,** *114* (8), 4041-4062.
(20) Stiefel, E. I., Proposed Molecular Mechanism for the Action of Molybdenum in Enzymes: Coupled Proton and Electron Transfer. *Proc. Nat. Acad. Sci.* **1973,** *70* (4), 988-992.
(21) Chen, G.-F.; Cao, X.; Wu, S.; Zeng, X.; Ding, L.-X.; Zhu, M.; Wang, H. Ammonia Electrosynthesis with High Selectivity Under Ambient Conditions via A Li^+ Incorporation Strategy. *J. Am. Chem. Soc.* **2017,** *139* (29), 9771-9774.
(22) Suryanto, B. H. R.; Kang, C. S. M.; Wang, D.; Xiao, C.; Zhou, F.; Azofra, L. M.; Cavallo, L.; Zhang, X.; Macfarlane, D. R. A Rational Electrode-Electrolyte Design for Efficient Ammonia Electrosynthesis Under Ambient Conditions. *ACS Energy Lett.* **2018,** *3* (6), 1219-1224.
(23) Zhou, F.; Azofra, L. M.; Ali, M.; Kar, M.; Simonov, A. N.; Mcdonnell-Worth, C.; Sun, C.; Zhang, X.; Macfarlane, D. R. Electro-Synthesis of Ammonia from Nitrogen at Ambient Temperature and Pressure in Ionic Liquids. *Energy Environ. Sci.* **2017,** *10*, 2516-2520.
(24) Voiry, D.; Fullon, R.; Yang, J.; De Carvalho Castro E Silva, C.; Kappera, R.; Bozkurt, I.; Kaplan, D.; Lagos, M. J.; Batson, P. E.; Gupta, G. *et al.* The Role of Electronic Coupling Between Substrate and 2D Mos_2 Nanosheets in Electrocatalytic Production of Hydrogen. *Nat Mater* **2016,** *15*, 1003.
(25) Paul, J.-F.; Payen, E. Vacancy Formation on MoS_2 Hydrodesulfurization Catalyst: DFT Study of the Mechanism. *J. Phys. Chem. B* **2003,** *107* (17), 4057-4064.
(26) Tsai, C.; Li, H.; Park, S.; Park, J.; Han, H. S.; Nørskov, J. K.; Zheng, X.; Abild-Pedersen, F. Electrochemical Generation of Sulfur Vacancies in the Basal Plane of Mos_2 for Hydrogen Evolution. *Nat Commun.* **2017,** *8*, 15113.
(27) Le, D.; Rawal, T. B.; Rahman, T. S., Single-Layer MoS_2 With Sulfur Vacancies: Structure and Catalytic Application. *J. Phys. Chem. C* **2014,** *118* (10), 5346-5351.
(28) Voiry, D.; Salehi, M.; Silva, R.; Fujita, T.; Chen, M.; Asefa, T.; Shenoy, V. B.; Eda, G.; Chhowalla, M. Conducting MoS_2 Nanosheets as Catalysts for Hydrogen Evolution Reaction. *Nano Lett.* **2013,** *13* (12), 6222-6227.
(29) Zhao, J.; Wang, X.; Xu, Z.; Loo, J. S. C. Hybrid Catalysts For Photoelectrochemical Reduction of Carbon Dioxide: A Prospective Review on Semiconductor/Metal Complex co-Catalyst Systems. *J. Mater. Chem. A* **2014,** *2* (37), 15228-15233.
(30) Li, S.-J.; Bao, D.; Shi, M.-M.; Wulan, B.-R.; Yan, J.-M.; Jiang, Q. Amorphizing of Au Nanoparticles by CeO_x–RGO Hybrid Support Towards Highly Efficient Electrocatalyst for N_2 Reduction Under Ambient Conditions. *Adv. Mater.* **2017,** 29 (33), 201700001.

(31) Shi, M.-M.; Bao, D.; Wulan, B.-R.; Li, Y.-H.; Zhang, Y.-F.; Yan, J.-M.; Jiang, Q. Au Sub-Nanoclusters On TiO_2 Toward Highly Efficient and Selective Electrocatalyst for N_2 Conversion to NH_3 at Ambient Conditions. *Adv. Mater.* **2017,** *29* (17), 1606550

(32) Lv, C.; Yan, C.; Chen, G.; Ding, Y.; Sun, J.; Zhou, Y.; Yu, G. An Amorphous Noble-Metal-Free Electrocatalyst Enables N_2 Fixation Under Ambient Conditions. *Angew. Chem. Int. Ed.* **2018**, 57 (21), 6073-6076.

(33) Azofra, L. M.; Sun, C.; Cavallo, L.; Macfarlane, D. R. Feasibility Of N_2 Binding and Reduction to Ammonia on Fe‐Deposited MoS_2 2D Sheets: A DFT Study. *Chem. Europ. J.* **2017,** *23* (34), 8275-8279.

(34) Kitano, M.; Kanbara, S.; Inoue, Y.; Kuganathan, N.; Sushko, P. V.; Yokoyama, T.; Hara, M.; Hosono, H. Electride Support Boosts Nitrogen Dissociation over Ruthenium Catalyst and Shifts the Bottleneck in Ammonia Synthesis. *Nat Commun.* **2015,** *6*, 6731.